Uncertainties, complexities and possible forecasting of the volcán de Colima energy emissions (México, years 2013-2015) based on the fractal reconstruction theorem.

Xavier Lana[1], Marisol Monterrubio-Velasco[2], Raúl Arámbula-Mendoza[3]

5 [1]Department of Physics, ETSEIB, Universitat Politècnica de Catalunya, Diagonal 647, 08028 Barcelona, Spain
[2]Department of Earth Sciences, Supercomputing Center, BSC-CNS, Eusebi Güell 1-3, 08034 Barcelona, Spain
[3]Centro Universitario de Estudios e Investigaciones de Vulcanología (CUEIV), Universidad de Colima, Av. Bernal Díaz del Castillo No. 340, Col. Villas San Sebastián, C.P. 28045, Colima, México

Correspondence to: Xavier Lana (francisco.javier.lana@upc.edu)

10 **Abstract.** A time series of effusive-explosive volcanic emissions of energy by the volcanic activity in Volcán de Colima (Western segment of Trans-Mexican volcanic belt, years 2013-2015) is analysed from the point of view of the reconstruction theorem, being considered several fractal computational procedures, such as the Hurst exponent (persistence, anti-persistence or randomness of the series), Lyapunov exponents and Kaplan-Yorke dimension (degree of forecasting difficulty on the series of energy emissions) and the correlation integral of the series, being obtained the Kolmogorov entropy and the embedding dimension (quantification of the degree of complexity and "loss of memory" of the physical mechanism along an episode of volcanic emissions). The analysed series have been chosen by applying the Gutenberg-Richter law to the logarithm of the complete energy emissions, being discarded those not accomplishing the mentioned law. Definitively, a series of 6182 explosive events and its seismic energy along years 2013-2015 has been selected. The reconstruction theorem algorithm is applied to the whole emission series, to 6 consecutive segments of 1000 emissions and to 21 moving window series of 2000 data lengths and shifts of 200 data, being also introduced and validated some examples of a nowcasting strategy. The main objective of this paper is to quantify the complexities concerning the physical and mathematical mechanisms governing these emissions, which are necessary for possible forecasting of explosive volcanic energy emissions with an enough degree of certainty.

1 Introduction

25 A right forecasting of dangerous long drought episodes, high magnitude earthquakes or great volcanic emissions should be one of the main objectives on the scientific fields of climatology, seismology or volcanology to prevent disasters which could affect the environment and the human life. Several examples of forecasting algorithms could be cited, among them the nowcasting strategy (Rundle et al., 2016, 2017), the multifractal analysis in seismology (Monterrubio-Velasco et al., 2020), the ARIMA process in climatic research (Lana et al, 2021), and neural algorithms (Lipton et al, 2015 and Lei, 2021) also

30 useful to predict monthly rainfall. Whereas the nowcasting strategy quantify the probability of an imminent extreme situation

(for instance a ~~high~~ magnitude earthquake), the other ~~cited~~ algorithms systematically forecast the next episode taking into account a certain number of previous recorded data, being this number strongly associated with the characteristics of the physical ~~mechanism.~~ These forecasting processes should be also validated by analysing the degree of complexity and the "loss of memory" of the physical mechanisms along the evolution of the physical process. In other words, how many

35 previous data would be necessary for a right use of the algorithm and which could be the range of uncertainties on the predictions. The database analysed, a time series of explosive volcanic events (Vulcanian explosions; Arámbula-Mendoza et al., 2018) emitted by Volcán de Colima (Western segment of Trans-Mexican volcanic belt, years 2013-2015) is detailed in Section 2. A Vulcanian explosion is an eruption in where fragmented material is expulsed to the atmosphere, as result of an overpressure into the conduit or lava dome. This event ~~release~~ energy in many ways, as elastic energy, seismic energy,

40 acoustic and thermal energy. The next explosion will occur when again the overpressure break again the impermeable cap. The Volcán de Colima in its recent past has experiment many Vulcanian explosions, some of them with generation of Pyroclastic Density Currents (PDCs) until 5 km of runout (Arámbula-Mendoza et al., 2019). Is for this reason that is important its study and analysis. The statistical distribution of these emissions and their return period ~~values~~ are described in the same section. The necessary ~~factors~~ (complexity, uncertainty and "loss of memory") to quantify the ~~certainty~~ of a

45 forecasting process are verified by means of the reconstruction theory (Diks, 1999) explained in Section 3. The results obtained after applying the reconstruction theorem, analysing the whole time series, 6 consecutive segments and 21 moving window data, are detailed in Section 4. Some examples of nowcasting are described in Section 5 and the most relevant results of the reconstruction theorem and their effects on forecasting algorithms are discussed in Section 6. Finally, the Conclusions, Section 7, summarize the most relevant results with respect to the expected success of forecasting algorithms

50 for the analysed volcanic series.

2. Database

A time series of volcanic explosions, know as Vulcanian explosions (Bachtell Clarke and Esposti Ongaro, 2015) emitted by Volcán de Colima (Western segment of Trans-Mexican volcanic belt, years 2013-2015) (Arámbula-Mendoza et al., 2018) is analysed from the point of view of the reconstruction theorem, with the aim of detecting the degree of difficulty ~~for~~ future

55 forecasting of volcanic emissions associated with energies close to or exceeding 10^8 ~~Joules~~. Figure 1a depicts the histogram of the logarithm of the emitted energy and Figure 1b the plot of emissions accomplishing the Gutenberg-Richter law, consisting in 6182 data with emissions equalling to or exceeding approximately 2×10^6 J.

Figure 2a describes the six segments to be analysed, where can be observed the highest explosions at the beginning of the first segment [$\log_{10}$(Energy)=8.2], third segment [$\log_{10}$(Energy)=8.4] and at the end of the series, out of the 6th segment

60 [$\log_{10}$ (Energy)=8.9]. With the aim of analysing the whole set of volcanic emissions accomplishing the Gutenberg-Richter law, Figure 2b depicts two examples of moving window segments, the second one, at the end of the data series, including the mentioned highest emission.

With respect to Figure 1a, some signs of a possible Gaussian distribution could be assumed. Nevertheless, a statistical analysis of these emissions, by means of the L-Skewness-Kurtosis formulation (Hosking and Wallis, 1997), shows that the

65   complete series of emissions, including those not accomplishing the Gutenberg-Richter law, are well fitted to the Generalised Logistic, GLO, function (Figure 3a and 3b). Additionally, three different empirical distributions of extreme emissions, equalling to or exceeding respectively 90%, 95% and 99% of empiric data (Figure 3b), can be associated with the Generalised Extreme value, GEV, function. Figure 4, shows the evolution of these three expected extreme emissions with the increasing return periods (given in number of events equalling to or exceeding 90, 95 and 99% respectively). It is

70   remarkable the fractal structure of these three extreme energy episodes, in spite of some departures of this power law within the interval of the highest return periods (especially for the 99% extreme distribution). For instance, the expected values of emissions for the three percentage levels and return periods up to 200 extreme emissions fit quite well the theoretical evolution, with emissions close to 1.0×10^8 J, 2.0×10^8 J and 8.0×10^8 J for 90, 95 and 99% extreme distributions. This first approach to the possibility of very high explosions and the corresponding expected return period (number of extreme

75   episodes before a very high extreme emission) would be quite similar to a nowcasting of the volcanic emissions of the Volcán de Colima structure. This strategy based on extreme episodes and return periods could depict some similarity to strategies proposed by Rundle et al. (2016, 2017) to detect the risk of imminent high magnitude earthquakes.

3. The reconstruction theorem

Previously to the reconstruction theorem (Diks, 1999) based on monofractal theory, the degree of randomness, anti-

80   persistence or persistence of the analysed data is established taking into account the concept of the Hurst exponent (Turcotte 1997) which is defined as the exponent H of the power-law

$$\frac{R(\tau)}{S(\tau)} \propto \tau^H,$$ (1)

85   being R(τ) the range of the different chosen segments of length τ of a series and S(τ) the corresponding standard deviation. H close to 0.5 implies a strong randomness of the series. Conversely, H clearly lowering or exceeding 0.5 means anti-persistence or persistence, respectively. Consequently, the Hurst exponent offers a first point of view of the behaviour of the analysed series. It has to be also remembered that the Hurst exponent has to be coincident with a specific value of the generalised Hurst exponent, obtained by means of multifractal analysis (Kantelhardt et al., 2002) applied to the same series.

90   The analysis of the monofractal structure of a series, by means of the reconstruction theorem (Diks, 1999), permits quantifying its complex forecasting by means of the following parameters:

-The necessary minimum number of nonlinear equations governing the physical mechanism, usually referenced as correlation dimension, μ(m), being m the reconstruction space dimension.

-The embedding dimension, d_E, the asymptotic value of the correlation dimension, with m theoretically tending to 0.

95   -The Kolmogorov entropy, κ, which quantifies the loss of memory of the mechanism along the physical process analysed.

The reconstruction theorem process is based on generating a set of m-dimensional space vectors using the series {x(i)} of data :

$$Z(i) = x_i, x_{i+1}, \ldots, x_{i+m-1}, i = 1, \ldots, n-m+1 \tag{2}$$

100

being n the length of the series, and the definition of the correlation integral in terms of the Grassberger–Procaccia formulation (Grassberger and Procaccia, 1983a, 1983b)

$$C(m,r) = \lim_{N \to \infty} \frac{1}{N^2} \sum_{i,j=1}^{N} H\{r - \|z(i) - z(j)\|\} \tag{3}$$

105

 r being an Euclidean distance in the m-dimensional space and H{.} the Heaviside function. The correlation integral can be rewritten as

$$C(m,r) = A_m e^{-mk} r^{\mu(m)} \tag{4}$$

110    $$\log\{C(m,r)\} = \log(A_m) - mk + \underline{(m)} \log(r) \tag{5}$$

being K the Kolmogorov entropy exponent and A_m and $\mu(m)$ the correlation amplitude and the mentioned correlation dimension for every reconstruction dimension m. A confident quantification of $\mu(m)$ for every reconstruction dimension has to be carefully computed, avoiding a very flat evolution of C(m,r) for small values of r, caused by ~~the~~ lacunarity (Turcotte,

115   1997), and ~~the~~ saturation of C(m,r) for the highest values of r. With respect to the quantification of the Kolmogorov entropy, K, by using equation 5, naming $\mu(m)$ the term $log\{C(m, r)\} - \mu(m)log(r)$, and after obtaining $\alpha(m)$, the equation 5 becomes

$$\alpha(m) = \log(A_m) - mK \tag{6}$$

120   Equation 6 is characterised by an almost constant value of $\log(A\underline{m})$ for high reconstruction dimensions m. Consequently, a very accurate value of the Kolmogorov coefficient K could be obtained by a linear regression in terms of equation 6, but only for the mentioned set of the highest reconstruction dimensions m. The same set of m-dimensional space vectors permits the computation of the Lyapunov exponents λ_i, (i=1,…m) (Eckmann et al., 1986; Stoop and Meier, 1988; Wiggins, 2003) which quantify the degree of uncertainty (specially the first λ_1 exponent) when the results, forthcoming volcanic emissions at the

125 present case, have been estimated by means of some forecasting algorithm. Additionally, the Kaplan-Yorke dimension, D_{KY}, (Kaplan and Yorke, 1979)

$$D_{KY} = l_0 + \left| \frac{1}{\lambda_{l0+1}} \right| \sum_{j=1}^{l_0} \lambda_j \qquad (7)$$

130 , with l_0 the maximum number of Lyapunov exponents in decreasing order accomplishing

$$\lambda_1 + \lambda_2 + ... + \lambda_{l_0} \geq 0, \qquad (8)$$

quantifies the fractal dimension of the nucleus around ~~of~~ which the consecutive m-dimensional vectors describe the
135 corresponding orbital trajectories. In short, the highest the value of D_{KY}, more complex will be to establish the forthcoming value of the analysed physical problem.

4. Results

4.1 The Hurst exponent.

The results of the Hurst exponent for the whole series and the six data segments is described in Figures 5a and 5b, being
140 obtained a clear sign of persistence for the complete series of Vulcanian explosions, with H exceeding a value of 0.7, a moderate persistence for the first, second, fourth and fifth segments, a smooth increase of H from the fifth to the sixth segment and a clear persistence (H > 0.70) for the third segment. This third clear persistence is detected for a data segment including the second highest energy emission (Figures 2a and 2b). Conversely, the lowest Hurst exponents for the

145 first, second, fourth and fifth segments are characterised by more moderate emissions of energy. Finally, the increase of H for the sixth segment could be caused by the imminence of the highest energy, an emission immediately after this data segment. A more detailed evolution of the Hurst exponent is described by the 21 moving windows (Figures 6a and 6b), being detected that the increasing of the persistence for the 6 first moving windows is stabilised for the other 15 windows with notable signs of persistence, with H varying from 0.72 to 0.76. In short, the factor of persistence from the point of view of
150 the Hurst exponent suggests a certain facility of forecasting algorithms, being remarkable that after the first 1000 emissions, (beginning of the five moving window), the highest persistency with some fluctuations is achieved and the highest emissions are included in these windows.

4.2 Embedding dimension.

155 With respect to the embedding dimension, Figure 7 illustrates five examples of the first segment of 1000 recorded emissions, where the slope, $\mu(m)$, of the $\log_{10}\{C(r)\}$ with respect to $\log_{10}\{r\}$ systematically increases for an interval of r, being then

described the asymptotic evolution of these slopes towards the definitive embedding dimension d_E. The embedding dimensions for the 21 moving windows and the 6 segments are respectively summarised in Table 1 and Table 2. By remembering that this dimension defines the minimum number of non-linear differential equations associated with the physical process, the most complex segments from the mathematical point of view would be the first, second, third and sixth, being not so complex the fourth and fifth ones. Nevertheless, the discrepancies when comparing the different segments are not excessive, given that 9 or 10 differential equations would be sufficient to analyse ~~every~~ one of the 6 segments. A quite different evolution of d_E is obtained for the 21 moving windows (Table 1), with dimensions approximately varying from 9.5 to 6.9. Between the 11th and 13th moving windows d_E diminishes (a more simplified mathematical structure should be assumed for these volcanic emissions) and for the remaining windows (14th -21th) their mathematical structures complexity roll back to moderate values (7.3 – 7.6).

4.3 The Kolmogorov entropy.

The obtained values of the Kolmogorov entropy exponent, based on equation 6 and summarised in Tables 1 and 2, are also illustrated with some examples (Figure 8). In these four ~~examples~~, the "loss of memory" of the physical mechanism is quite similar for the 6th segment and the 10th moving window, with values of $\underline{K}$ which could complicate a bit more the forecasting processes, in comparison with the previous 5th segment and the 13th moving window. In spite of these discrepancies with respect to the "loss of memory" for the different segments and moving windows, they are quite similar in many cases, being only remarkable two examples of extreme minimum (fifth segment, $\underline{K}$ =0.258) and extreme maximum (10th moving window, $\underline{K}$ = 0.410). Consequently, the "loss of memory", making complex the forecasting process, would not affect in the same way to all the volcanic explosive emissions.

4.4 The Lyapunov exponents.

A right computation of the Lyapunov exponents needs an iterative process, with the aim of minimising the final uncertainty on every exponent. At the present computations, 975 iterations have been good enough to obtain the first fifteen exponents with very small oscillations at the end of the iterative process. An example of this process is shown in Figure 9, where are described the evolution of the exponents for the third segment of emissions up to λ_{15}. A higher number of exponents is not necessary by two ~~questions~~. First, the possible errors or uncertainties on forecasting processes could be specially associated with the first Lyapunov exponents. Second, observing the evolution at the end of iterations of the exponents of Figure 9, the Kaplan-Yorke dimension ~~can be computed without the necessity of Lyapunov exponents exceeding dimension 15.~~

The results are summarised in Table 3, showing the mean and standard deviation for every one of the first ten Lyapunov exponents, obtained for the 21 moving windows and the six data segments after 975 iterations of the corresponding computational algorithm to obtain accurate and confident values. First, in agreement with the results exposed in the mentioned table, every one of the λ_i exponent is quite similar both for segments and moving windows, bearing in mind the

very similar average values and small standard deviations. Second, the first small negative Lyapunov values are always detected for λ_7 or λ_8. Consequently, the information offered by the Lyapunov exponents, concerning the possible errors on forecasting, should be very similar all along the emissions, being not detected differences between data segments and moving windows. Finally, the Kaplan-Yorke dimension also offers values manifesting again the notable similarity of the

195 Lyapunov structure for both segments and moving window.

Whereas for the six trams, D_{KY} varies from 12.51 to 12.75, the range is quite similar for the 21 moving windows, varying from 12.70 to 13.04. Consequently, the fractal dimension of the nucleus around which the consecutive m-dimensional reconstructed vectors describe the corresponding trajectories is complex (a fractal dimension exceeding 12.0). Nevertheless, this complexity becomes confined within a short interval, being quite similar for all segments and moving windows.

200

5. Some examples of nowcasting

The nowcasting process (Rundle et al., 2016, 2017) is based on the computation of the "natural time", or in other words, the number of consecutive earthquakes (seismic cycle length) with magnitudes within a determined interval. In this way, the empiric cumulative distribution function, CDF, of these "natural times" would be stablished by the high magnitude

205 earthquakes interrupting these seismic cycle lengths. Consequently, the nowcasting process does not exactly predict a forthcoming high magnitude, but quantify the probability of an imminent high earthquake magnitude, based on the CDFs curves.

A first illustrative example, from the point of view of the seismic activity, of the nowcasting algorithm is shown in Figure 10a. It corresponds to the recorded seismic activity in Canterbury (New Zealand, years 1970-2020). The minimum seismic

210 magnitude to construct several CDFs is 2.5 (minimum magnitude accomplishing the Gutenberg-Richter law) and three different maximum magnitudes are 4.5, 5.0 and 5.5 to obtain three different sets of cycle lengths. The probability of forthcoming extreme magnitudes (7.2 and 7.8) interrupting a cycle length exceeds 80%. Consequently, the probability of an earthquake of similar extreme magnitudes should be more or less imminent if the real cycling length is approximately ranging between 100 and 1000 "natural times", depending on the chosen maximum magnitude Mmax.

215 Two examples of nowcasting corresponding to volcanic energy explosions are shown in Figure 10b. The first one corresponds to the volcanic activity of the third segment (Figure 2a) and the second includes the whole series of volcanic emissions. In both cases, the cycle lengths are obtained by considering a minimum and maximum level of volcanic emission of, respectively, $10^{2.5}$ J and $10^{4.5}$ J.   Conversely to the example of seismic activity, the few extreme levels exceeding $\log_{10}(Energy) = 8.0$ are not associated with high CDF values. Consequently, the nowcasting algorithm could be considered

220 less effective in comparison with the seismic activity results, probably due to the mechanism of the volcanic emissions, which do not include structures such as background activity, swarms, forecastings, mainshocks and aftershocks. Nevertheless, a notable number of high $\log_{10}(Energy)$ emissions slightly smaller than 8.0, and some of them very close to the highest emissions, are associated with values of CDFs close to 0.6, and even exceeding 0.8. An example of this fact could be the third segment of emissions, where some of them are not independent but associated with the highest emission close to

225 8.5. In short, the nowcasting could be also assumed as an algorithm contributing to the predictability of volcanic explosions, but perhaps not so obvious as for the case of seismic activities.

6. Discussion of the results

The results obtained by the reconstruction theorem and the possible relationships between the fractal reconstructions
230 exponents (H, K, λ and d_E) and changes on the volcanic emissions are summarized in Figures 11a and 11b. First of all, relevant changes on parameters such as mean, standard deviation, skewness and kurtosis (Table 4) are not detected for the different segments of volcanic emissions. Additionally, the Kolmogorov-Smirnov test (95 and 99% of probability) discards the possible Gaussian distribution of these emissions, in agreement with Figures 3a and 3b, where the Generalised logistic distribution (GLO) is assumed bearing in mind the L-Skewness-Kurtosis formulation.

235 The Hurst exponent (Figure 11a) is characterised by a continuous ~~increasing,~~ finally achieving oscillations close to 0.7, with evident structure of persistence since the 7th up to the 21th moving window, all of them including two high emissions, $\log_{10}(energy) = 8.372$ and 7.937. Consequently, the values of Hurst would manifest persistence (convenient for appropriate forecasting) when a high emission becomes included in the moving window. Conversely, the "loss of memory" (Kolmogorov exponent) of the physical mechanism (not convenient for good forecasting) increases up to the 10th window,
240 notably decreasing for the rest of windows. In this case, the influence of a high emission would appear outdated in comparison with the results of the Hurst exponent. With respect to the Lyapunov exponent, λ_1, its changes along the moving windows are small (Figure 11a) with not very remarkable discrepancies with an average value of 0.169 and a standard deviation of 0.013 (Table 3). Consequently, the different forecasting errors on energy emissions could not be different, at least from the point of view of λ_1. These errors could be also consequence of the degree of complexity of the non-linear
245 differential equations system, quantified by the embedding dimension, d_E. Figure 11b depicts the clear reduction of this complexity after the 10th moving window, with a fast decrease up to the 13th window and values close to 7.5 after this last cited window. Similar to the evolution of the Kolmogorov entropy, close to the 10th window, an evident decrease of both fractal parameters is detected. Reinforcing this similarity, it is also noticeable the stabilised values of these two fractal parameters for the 13th and 14th windows. It is also convenient to observe that, in agreement with the very similar obtained
250 Kaplan-Yorke dimensions (ranging from 12.5 to 13.0) for segments and moving windows, the data-vectors of high dimension m used for the reconstruction theorem, depict a very similar structure. In other words, the trajectories of these reconstructed vectors around the fractal nucleus are quite similar.

With respect to the results of the nowcasting, the return period curves (90%, 95% and 99% of extreme emissions) could be,
255 as cited before, a strategy relatively similar. Nevertheless, the nowcasting process permits to decide minimum and maximum emission of energy levels to define the best ~~empiric~~ distribution of cycle lengths of "natural waiting time", detecting in this way the probability, in percentage, of a probable imminent volcanic emission of high energy. In spite of the nowcasting method does not determine a concrete next volcanic emission, given that it is not a forecasting process, it takes into account

that future high emissions will be expected with similar "natural waiting times". Although some emissions, (Figures 10b),
260   exceeding $\log_{10}$(Energy) = 7.5 have probabilities close to 50-60%, probabilities close to or exceeding 80% are also obtained.
In short, the nowcasting process seems to be more effective with seismic activity than volcanic emissions. Nevertheless, their
results could be also compatible and complementary with algorithms forecasting the high emission of volcanic energy.

7. Conclusions

265   The fractal parameters, obtained by means of the reconstruction theorem of 6 segments and 21 moving windows of the
analysed volcanic explosions in Volcán de Colima (México), as well as the nowcasting strategy, are the first steps for the
application of different forecasting processes. The next researches should prevent with respect to future emissions, especially
those of high energy, by means of several forecasting algorithms (Box and Jenkins, 1976; Lipton et al, 2015; Rundel et al.,
2017 and Lei, 2021, among others) and Multifractal analysis of moving window data (Monterrubio-Velasco et al., 2020). In
270   spite of the uncertainties with respect to the time of an emission and its corresponding energy, estimated by means of
forecasting, are expected to be non-negligible, these algorithms should depict reasonably good approaches to real energy
emissions bearing in mind the obtained reconstruction theory results. Additionally, the evolution of the multifractal structure
is expected to be a warning process for volcanic activities approaching to high emissions of energy, quite similar
(Monterrubio-Velasco et al., 2020) to the analysis of consecutive seismic magnitudes.

275

Competing interests

The contact author has declared that none of the authors has any competing interests

Acknowledgments

280   The research leading to these results has received funding from the European High-Performance Computing Joint
Undertaking (JU) and Spain, Italy, Iceland, Germany, Norway, France, Finland, and Croatia, under grant agreement No.
101093038, ChEESE-CoE

Data availability

285   Data sharing is not applicable to this article as no new data were created or analyzed in this study.

290

References

Arámbula-Mendoza, R., Reyes-Dávila, G., Vargas-Bracamontes, D. M., González-Amezcua M., Navarro-Ochoa, C., Martínez-Fierros, A., Ramírez-Vázquez, A. Ariel: Seismic monitoring of effusive-explosive activity and large lava dome collapses during 2013–2015 at Volcán de Colima, Mexico, J. Volcanol. Geotherm. Res., 351, 75-88, doi:10.1016/j.jvolgeores.2017.12.017, 2018.

Arámbula-Mendoza, R., Reyes-Dávila, G., Domínguez-Reyes, T., Vargas-Bracamontes, D., González-Amezcua, M., Martínez-Fierros, A., Ramírez-Vázquez, A: Seismic Activity Associated with Volcán de Colima. In Volcán de Colima, portrait of a Persistently Hazardous Volcan, doi:10.1007/978-3-642-25911-1_1, Ed. Springer, 2019.

Bachtell Clarke, A., Esposti Ongaro, Belousov T.: Vulcanian eruptions. The Encyclopedia of Volcanoes, Editor in chief, Haraldur Sigurdsson. Elsevier. Box, G.E.P. and Jenkins, G.M. (1976) Time Series Analysis: Forecasting and Control. CA: Holden-Day 575 pp., doi:10.1016/B978-0-12-385938-9.00028-6, 2015.

Diks, C.: Nonlinear time series analysis. Nonlinear Time Series and Chaos, vol. 4. World Scientific Edit., 209 pp. Doi: 10.1017/CBO9780511755798, 1999.

Eckmann JP, Oliffson S, Ruelle D, Cilliberto S.: Lyapunov exponents from time series, Phys. Rev. A., 34(6): 4971–4979, doi: 10.1103/PhysRevA.34.4971, 1986.

Grassberger P, Procaccia I.: Characterization of strange attractors. Physical Review Letters, 50, 346–349, 1983a.

Grassberger P, Procaccia I.: Estimation of the Kolmogorov entropy from a chaotic signal. Physical Review A, 28, 448–451, 1983b.

Hosking, J.R.M., Wallis, J.R.: Regional frequency analysis. An approach based on L-moments. Cambridge University Press, 224 pp, 1997.

Kantelhardt JW, Zschiegner SA, Koscielny-Bunde E, Havlin S, Bunde A, Stanley HE.: Multifractal detrended fluctuaction analysis of nonstationary time series. *Physica A, 316,* 87–114, 2002.

Kaplan JK, Yorke JA.: Chaotic behaviour of multidimensional difference equations. In *Functional Difference Equations and Approximation of Fixed Points*, Vol. 730, Walter HO, Peitgen HO (eds). Springer Verlag: Berlin, 204–227, 1979.

Lana, X., Rodríguez-Solà, R., Martínez, M.D., Casas-Castillo, M.C., Serra, C. and Kichner, R.: Autoregressive process of monthly rainfall amounts in Catalonia (NE Spain) and improvements on predictability of length and intensity of drought episodes. International Journal of climatology, 41, 3178-3194. doi.org/10.1002/joc.6915., 2021.

Lei, C.: RNN, Deep Learning and Practice with MindSpore. Springer Singapore, pp 83-93, 2021.

Lipton, Z.C, Berkowitz, J., Elkan, C.: A critical review of recurrent neural networks for sequence learning. arXiv preprint arXiv:1506.00019, 2015.

335 Monterrubio-Velasco, M., Lana, X., Martínez, M.D. Zúñiga, R. and de la Puente, J.: Evolution of the multifractal parameters along different steps of a seismic activity. The example of Canterbury 2000-2018 (New Zealand). American Institute of Physics. AIP Advances. Doi: 10.1063/5.0010103, 2020.

Rundle, J.B., Turcotte, D.L., Donnellan, A., Grant, Ludwig, L., Luginbuhl, M., Gong, G.: Nowcasting earthquakes. AGU
340 Publications. https://doi.org/10.1002/2016EA000185, 2016.

Rundle, J.B., Luginbuhl, M., Giguere, A., Turcotte, D.L.: Natural time, nowcasting and the physics of earthquakes: estimation of seismic risk to global megacities. Pure and Applied Geophysics.
DOI 10.1007/s00024-017-1720-x, 2017.

345

Stoop F, Meier PF.: Evaluation of Lyapunov exponents and scaling functions from time series. *J. Opt. Soc. Am. B* 5: 1037–1045, 19898

Turcotte DL.: Fractals and Chaos in Geology and Geophysics, 2nd edition. Cambridge University Press. Cambridge, UK,
350 398 pp, 1997.

Wiggins S.: Introduction to Applied Nonlinear Dynamical Systems and Chaos. Text in Applied Mathematics, Vol. **2**, 2nd edn. Springer, New York, NY, 843 pp, 2003.

355

360

a)

b)
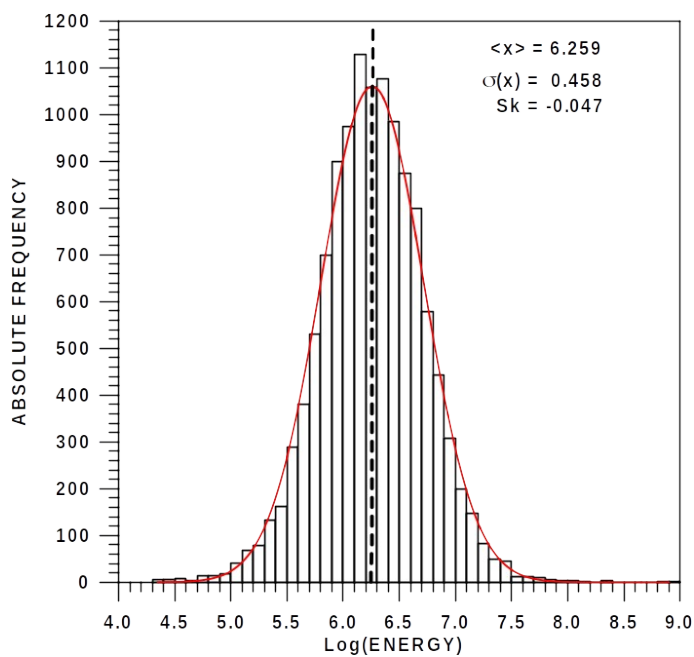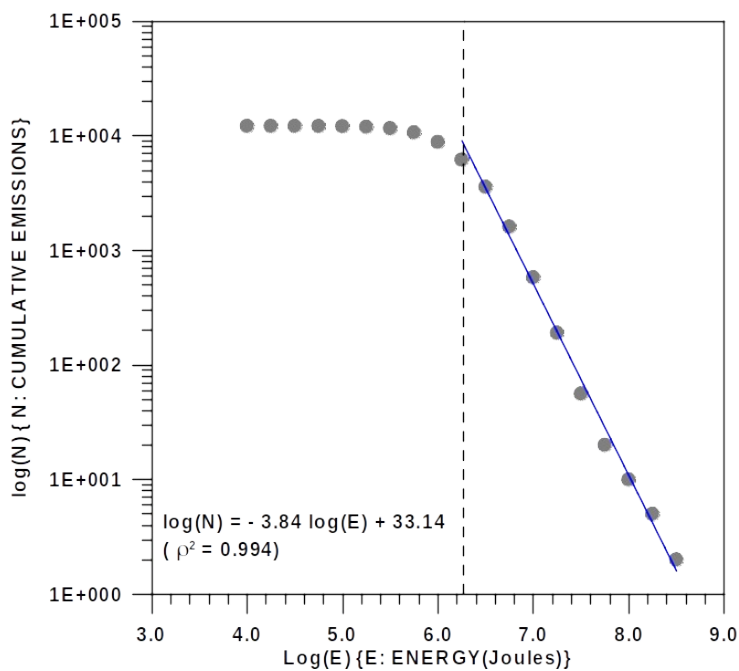
Figure 1. a) Histogram of the volcanic emission energies and b) logarithm of energies accomplishing the Gutenberg-Richter law.

a)
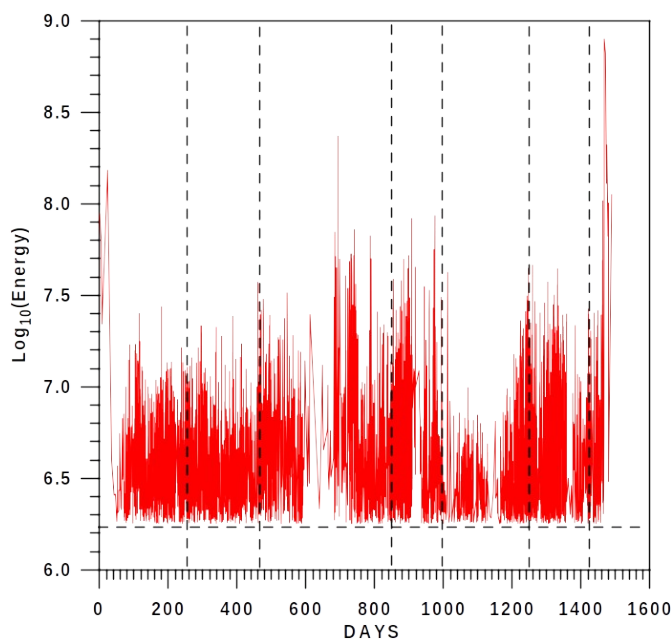
b)
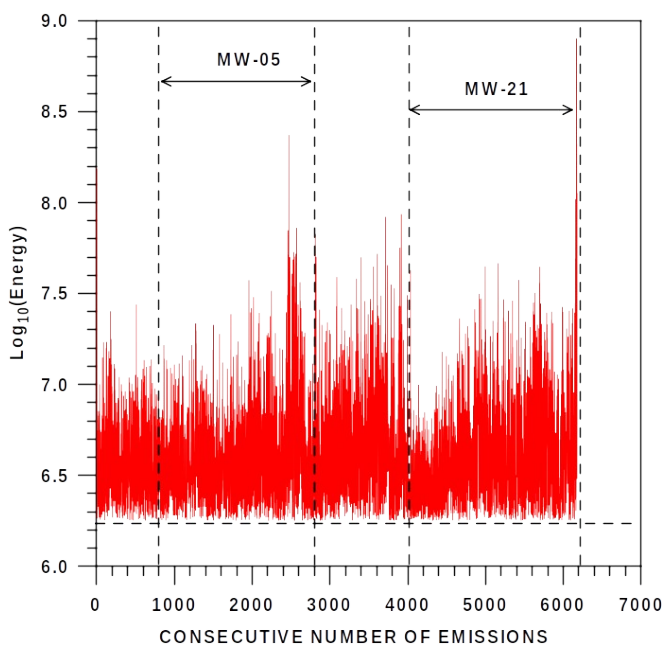
Figure 2. a) Evolution of the volcanic energy emission accomplishing the Gutenberg-Richter law. Vertical dashed lines define the segments (intervals of 1000 data) b) Two examples of dataset defined by moving windows of amplitude 2 thousand elements and shift of 200 positions.

a)
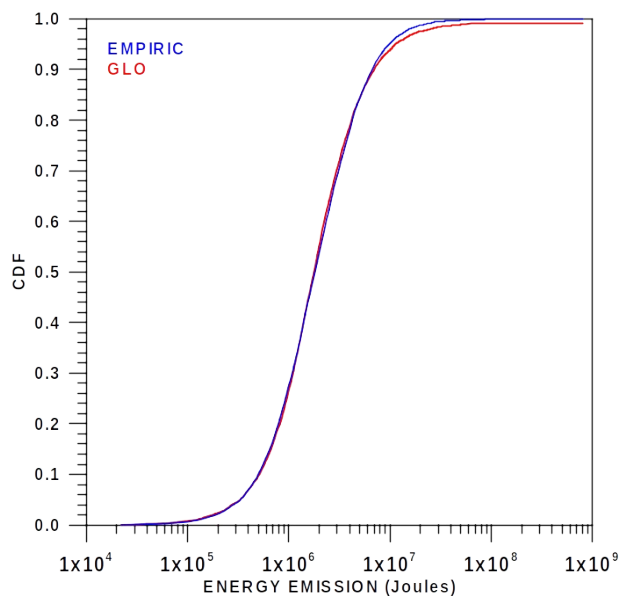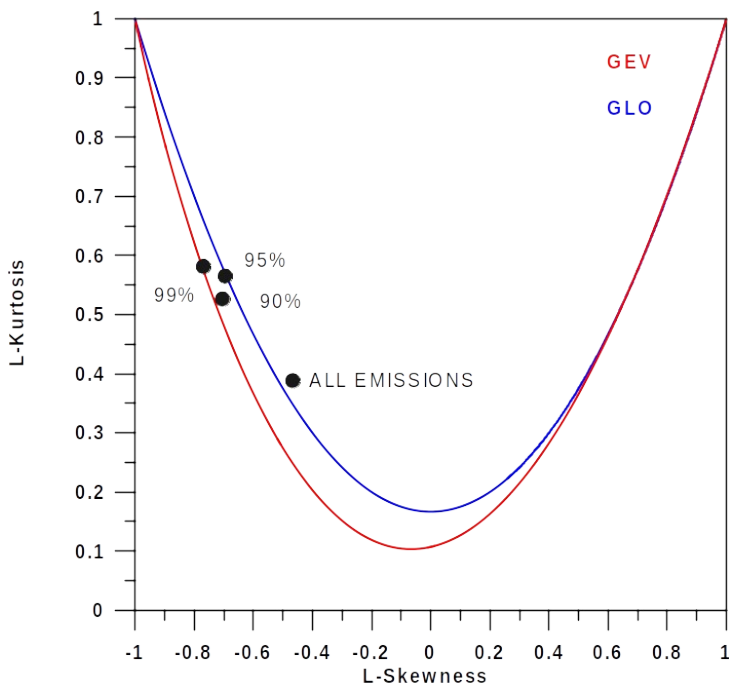
b)

Figure 3. **Cumulated distribution function of the effusive volcanic energy emissions. Empiric probabilities are well reproduced, bearing in mind the L-Skewness-Kurtosis formulation, by the GLO (generalised logistic distribution). Emissions equalling to or exceeding 90%, 95% and 99% could be associated with the GEV (generalised extreme values distribution).**

$$\log_{10}(E_r) = 0.620 \log_{10}(Tr) + 15.903 \quad (\rho^2 = 0.973)$$

EXTREME 90%

$$\log_{10}(E_r) = 0.581 \log_{10}(Tr) + 16.399 \quad (\rho^2 = 0.980)$$

EXTREMES (95%)

$$\log_{10}(E_r) = 0.738 \log_{10}(Tr) + 16.875 \quad (\rho^2 = 0.968)$$

EXTREMES (99%)
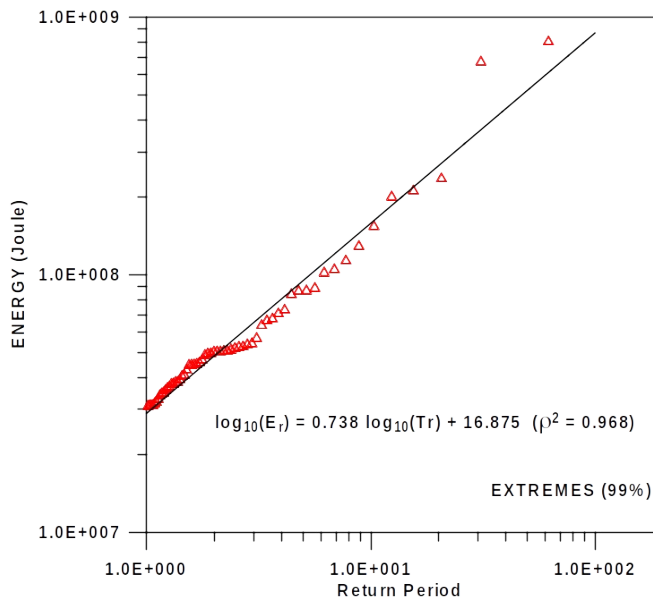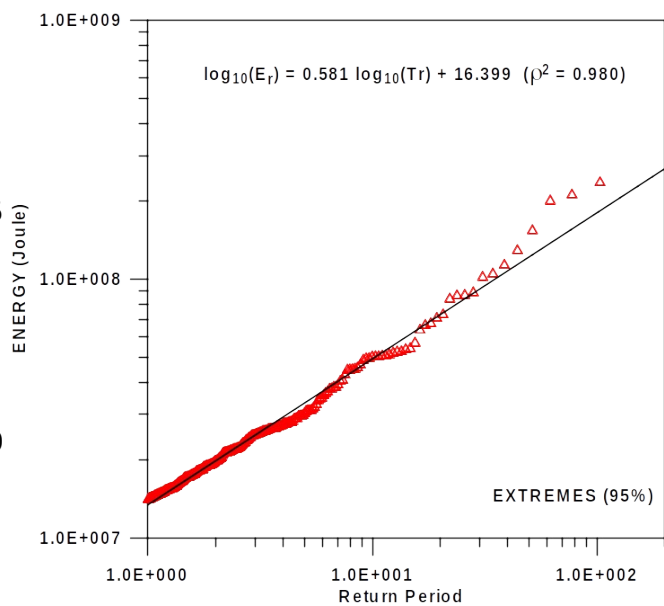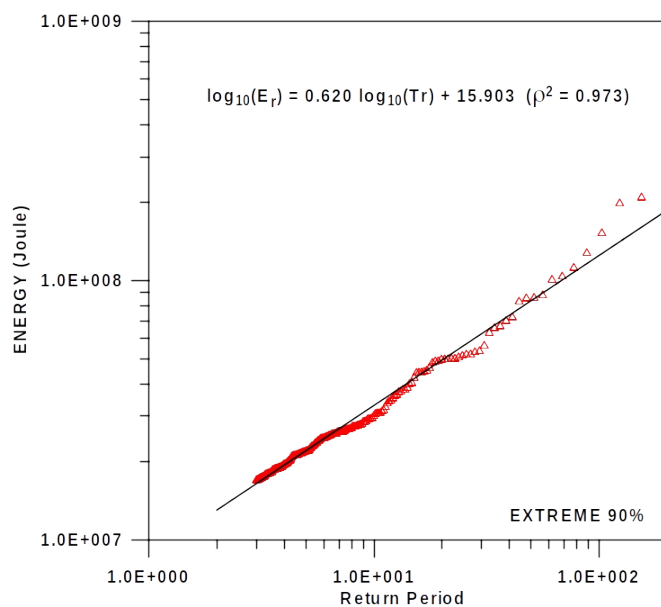
Figure 4. Return period curves (90, 95 and 99%) of extreme emissions.

a)

b)
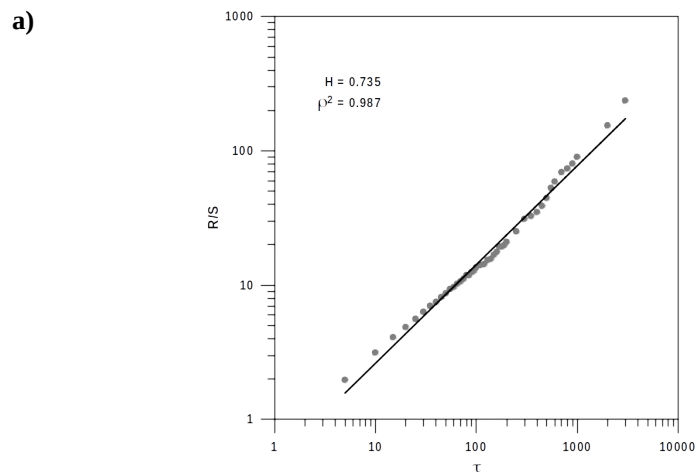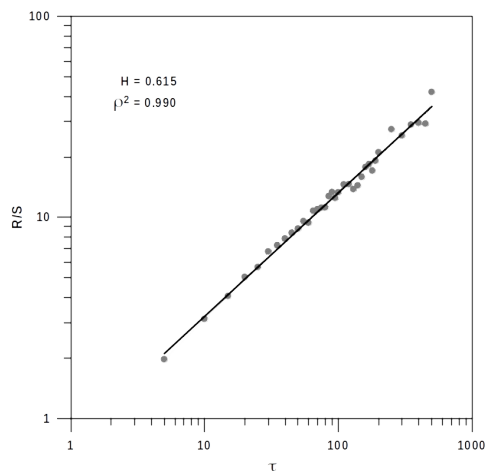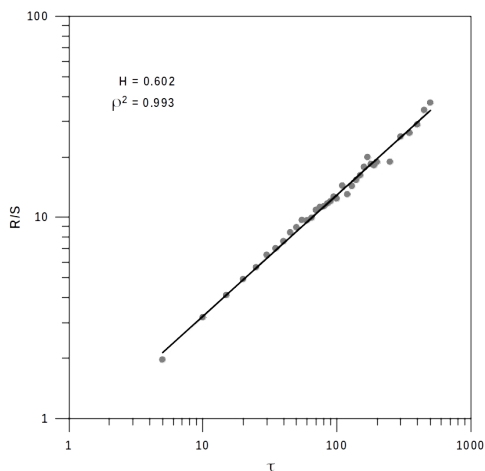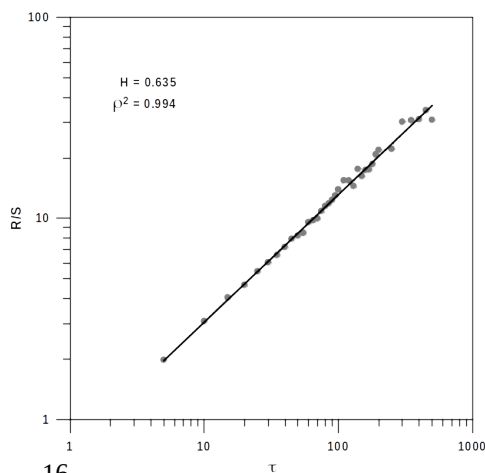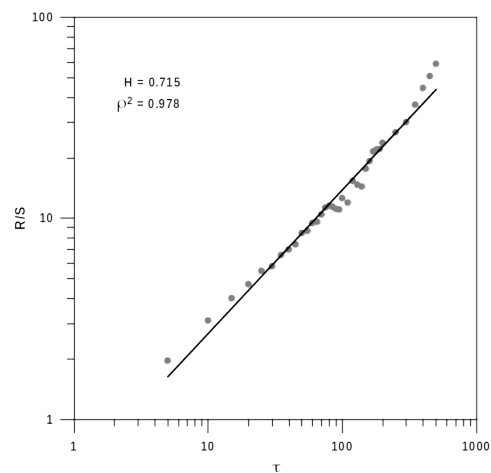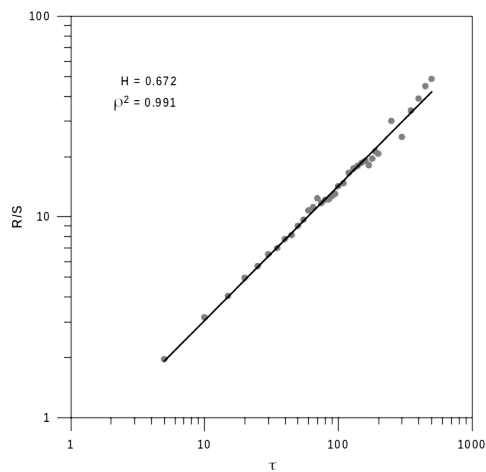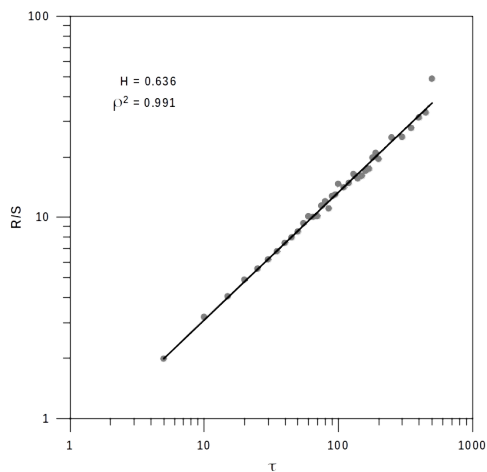
Figure 5. Hurst exponent for a) the whole series of effusive emissions of energy accomplishing the Gutenberg-Richter law and b) the same series fragmented on six trams of equal number of records.
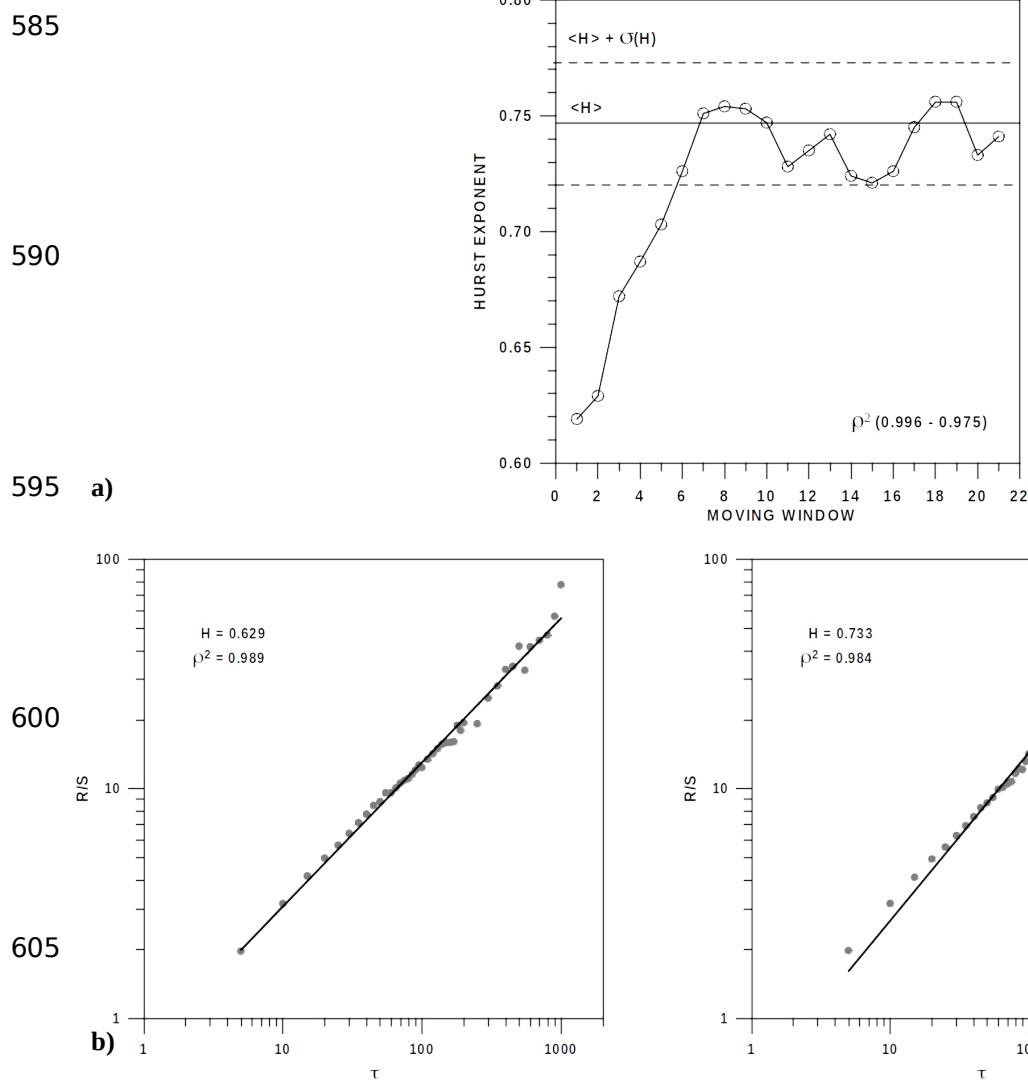
Figure 6. a) Evolution of the Hurst exponent for the 21 moving windows and b) two examples for windows 2 and 6

Figure 7. An example of the evolution of embedding dimension (first segment of 1000 elements) for reconstruction dimensions m = 2, 4, 8, 12, 16.
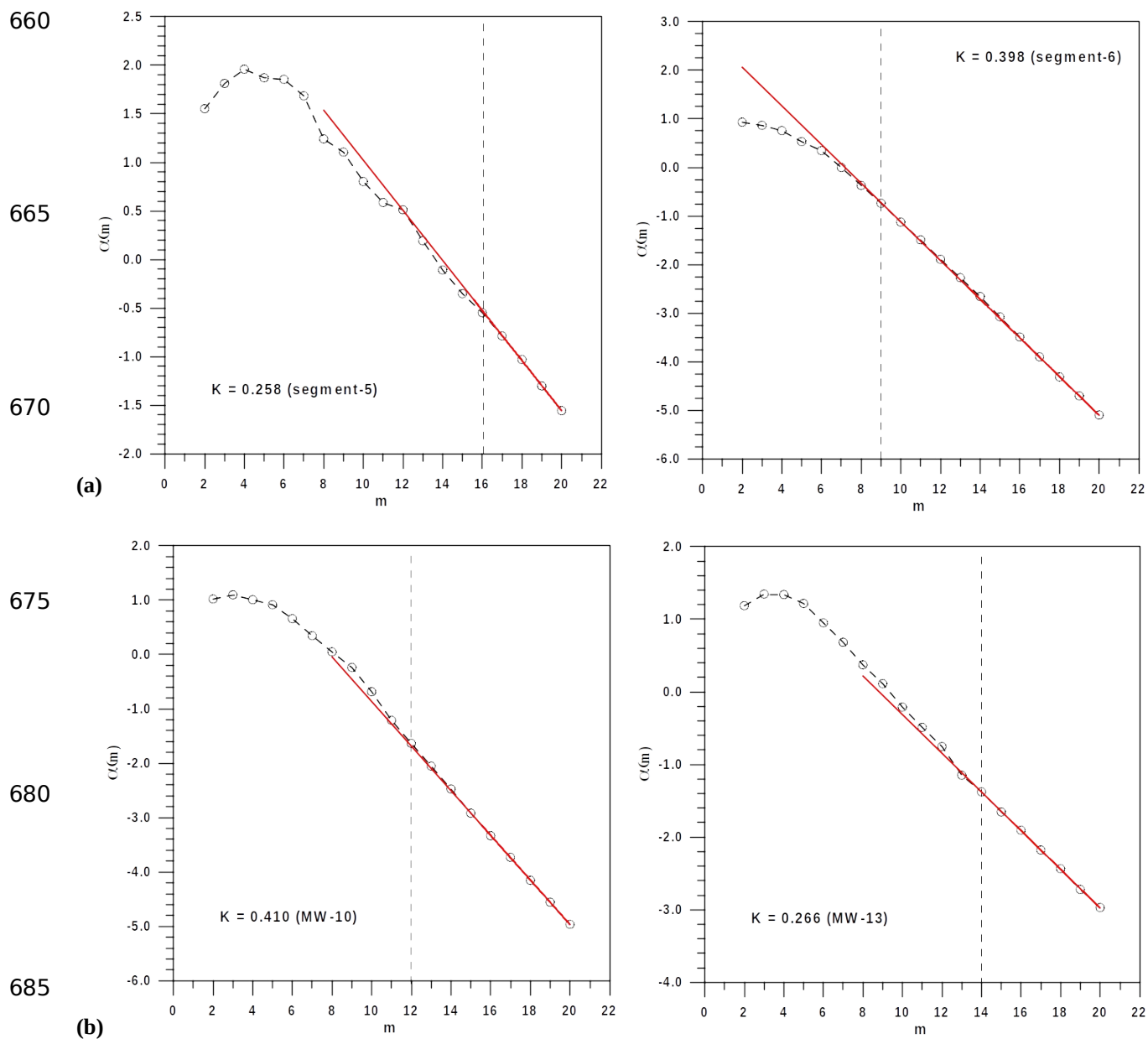
Figure 8. a) Two examples of Kolmogorov exponents for two segments of 1000 elements and b) two examples for moving windows.

695

700

705
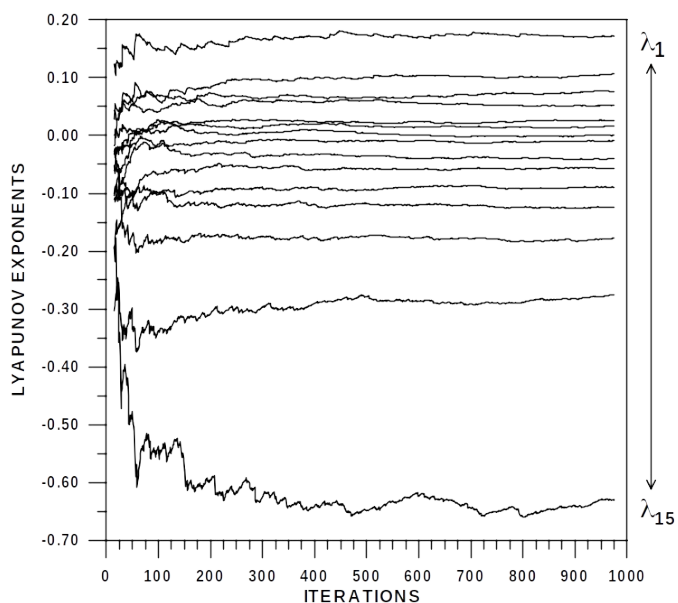
Figure 9. Fifteen Lyapunov exponents for the third segment of the effusive-explosive volcanic emissions.

710

715

720

725
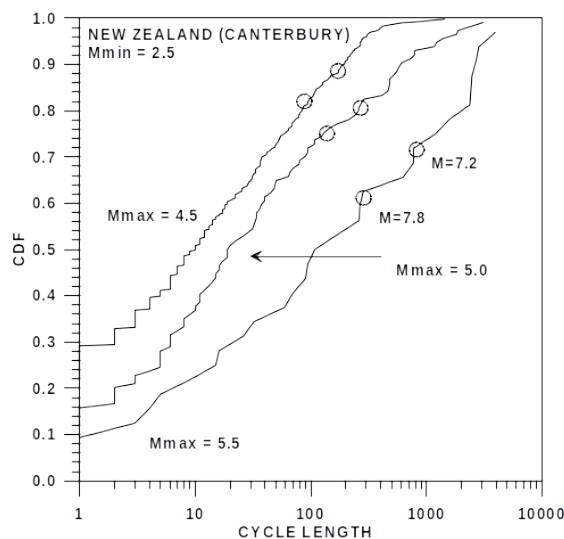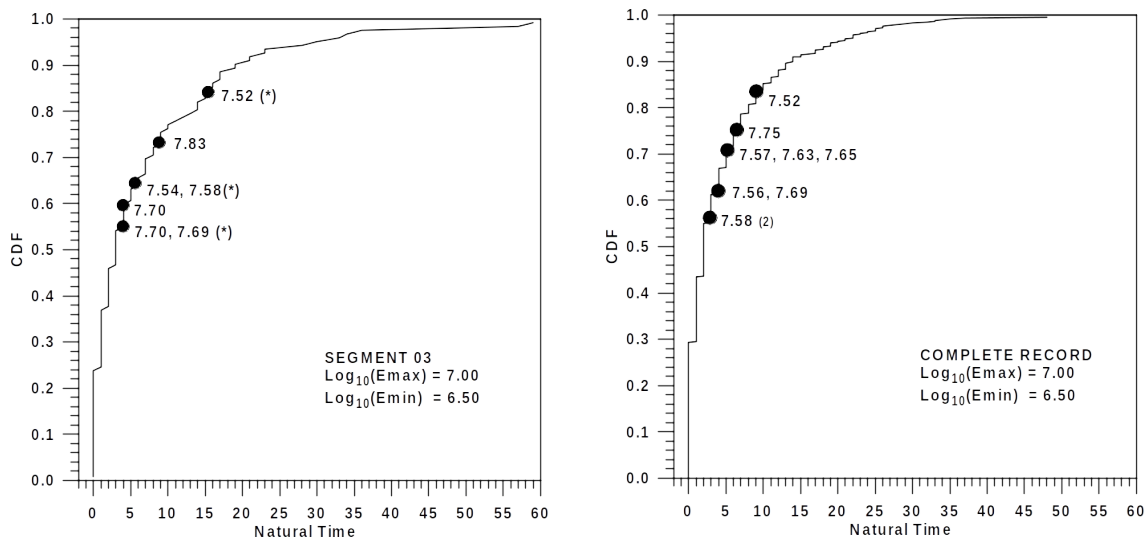
Figure 10. A comparison of nowcasting for a) the seismic activity of Canterbury (New Zealand), 1990-2021 and the energy of the volcanic emissions of Colima (México), 2013-2015. b) The third segment and c) the whole series of volcanic emissions of energy. Log₁₀(energies) with asterisk in figure b) correspond to those also detected by using the complete volcanic record in figure c).

765

780
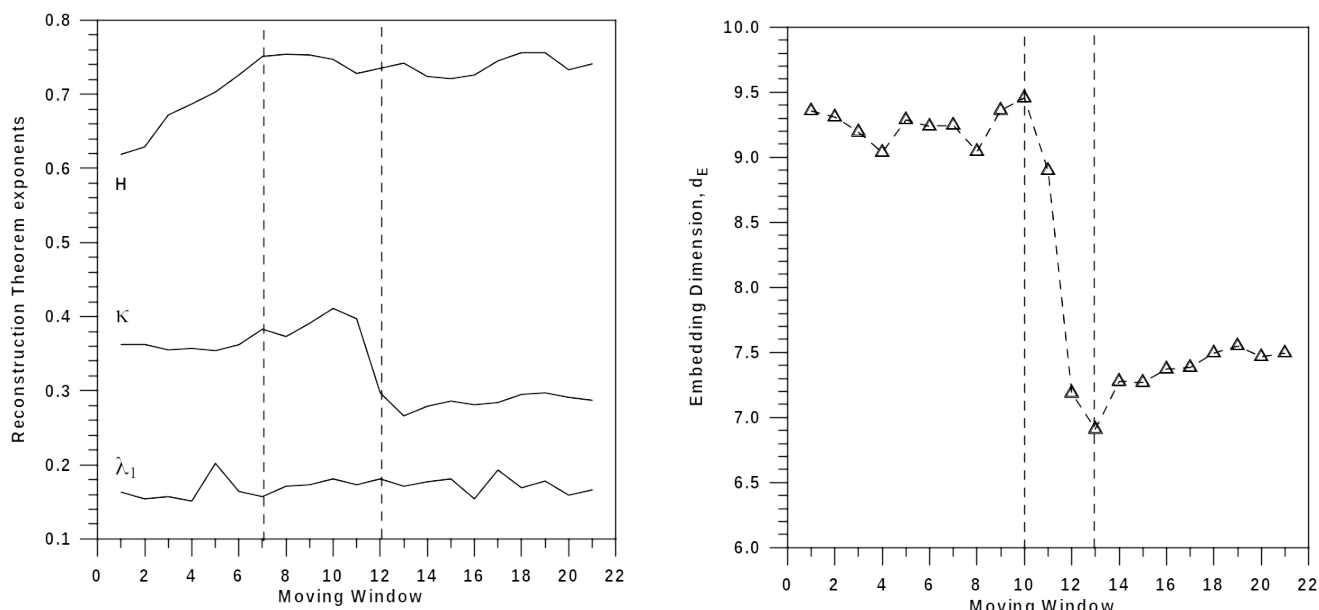
Figure 11. a) Evolution of the Hurst, H, Kolmogorov, *K*, and first Lyapunov exponent, λ_1. b) Embedding dimension d_E, for the 21 moving windows.

MW	1	2	3	4	5	6	7	8	9	10	11
d_E	9.356	9.309	9.195	9.037	9.287	9.237	9.246	9.044	9.361	9.456	8.898
K	0.362	0.363	0.355	0.357	0.354	0.362	0.383	0.373	0.391	0.410	0.397
MW	12	13	14	15	16	17	18	19	20	21	
d_E	7.188	6.910	7.277	7.270	7.372	7.385	7.495	7.550	7.467	7.495	
K	0.297	0.266	0.279	0.286	0.281	0.284	0.295	0.297	0.291	0.287	

785

Table 1. Embedding dimension and Kolmogorov coefficient for the 21 moving windows.

SEGMENT	1	2	3	4	5	6
d_E	9.155	8.932	8.727	7.952	8.101	9.340
K	0.359	0.338	0.377	0.375	0.258	0.398

790   **Table 2.** Embedding dimension and Kolmogorov coefficient for the 6 segments of volcanic emissions.

SEGMENT	$\lambda 1$	$\lambda 2$	$\lambda 3$	$\lambda 4$	$\lambda 5$	$\lambda 6$	$\lambda 7$	$\lambda 8$	$\lambda 9$	$\lambda 10$
$\langle\lambda\rangle$	0.156	0.105	0.074	0.053	0.032	0.015	-0.001	-0.018	-0.039	-0.062
$\sigma(\lambda)$	0.011	0.004	0.005	0.004	0.003	0.003	0.004	0.005	0.003	0.004

Table 3. Mean and standard deviation for the first ten Lyapunov exponents, after 975 iterations.

795

SEGMENT	0001-6182	0001-1000	1001-2000	2001-3000	3001-4000	4001-5000	5001-6000	6001-6182
MAXIMUM	8.903	8.187	7.574	8.372	7.937	7.650	7.667	8.903
MEAN	6.610	6.578	6.563	6.641	6.663	6.558	6.633	6.730
ST.DEV	0.283	0.233	0.225	0.313	0.310	0.242	0.292	0.470
SKEWNESS	1.394	1.252	0.931	1.267	1.035	1.144	0.834	2.085
KURT0SIS	3.462	3.695	0.780	2.033	1.016	1.328	0.110	5.394
K-S TEST	0.102	0.081	0.083	0.106	0.091	0.102	0.095	0.154
K-S_0.05	0.017	0.043	0.043	0.043	0.043	0.043	0.043	0.100
K-S_0.01	0.021	0.051	0.051	0.051	0.051	0.051	0.051	0.120

Table 4. Basic characteristics of the energy emissions (logarithm of energy), for the whole database, the 6 segments of 1,000 elements and the last segment of 182 elements. The empirical results of the Kolmogorov-Smirnov, K-S, tests are compared with the significance levels of 95 and 99%, KS_0.05 and KS_0.01, corresponding to the Gaussian
800 **distribution.**